Predicting the 1-AU Arrival Times of Coronal Mass Ejections

Nat Gopalswamy, [1,2] Alejandro Lara, [3] Seiji Yashiro, [1,2] Mike L. Kaiser [2] and Russell A. Howard [4]

Abstract

We describe an empirical model to predict the 1-AU arrival of coronal mass ejections (CMEs). This model is based on an effective interplanetary (IP) acceleration described in Gopalswamy et al. [2000b] that the CMEs are subject to, as they propagate from the Sun to 1 AU. We have improved this model (i) by minimizing the projection effects (using data from spacecraft in quadrature) in determining the initial speed of CMEs, and (ii) by allowing for the cessation of the interplanetary acceleration before 1 AU. The resulting effective IP acceleration was higher in magnitude than what was obtained from CME measurements from spacecraft along the Sun-Earth line. We evaluated the predictive capability of the CME arrival model using recent two-point measurements from the Solar and Heliospheric Observatory (SOHO), Wind and ACE spacecraft. We found that an acceleration cessation distance of 0.76 AU is in reasonable agreement with the observations. The new prediction model reduces the average prediction error from 15.4 to 10.7 hrs. The model is in good agreement with the observations for high speed CMEs. For slow CMEs, the model as well as observations show a flat arrival time of ~4.3 days. Use of quadrature observations minimized the projection effects naturally without the need to assume the width of the CMEs. However, there is no simple way of estimating the projection effects based on the surface location of the Earth-directed CMEs observed by a spacecraft (such as SOHO) located along the Sun-Earth line because it is impossible to measure the width of these CMEs. The standard assumption that the CME is a rigid cone may not be correct. In

fact, the predicted arrival times have a better agreement with the observed arrival times when no projection correction is applied to the SOHO CME measurements. The results presented in this work suggest that CMEs expand and accelerate near the Sun (inside 0.7 AU) more than our model supposes; these aspects will have to be included in future models.

1. Introduction

While electromagnetic disturbances from the Sun travel to 1 AU in minutes, the Solar wind disturbances take a few days after originating at the Sun [Haurwitz, Yoshida and Akasofu, 1965; Cane, 1984; Vandas et al., 1996; Brueckner et al., 1998; Bravo and Blanco-Cano, 1998; Gopalswamy et al., 1998a]. The primary observational manifestation of the solar disturbances is the coronal mass ejection (CME) detected remotely by white-light coronagraphs. CMEs are also detected locally at 1 AU by spacecraft. Knowing the arrival time of CMEs at 1 AU accurately is of crucial importance in predicting space weather, because the severest of geomagnetic storms are caused by CMEs [see, e.g., Gosling, 1993]. Predictions based on remotely detected CMEs is the most practical way of getting advance warning of solar disturbances heading towards Earth. Unfortunately, we only have measurements of CME properties near the Sun and near Earth, so we have to make empirical models based on these two-point measurements. Some radio techniques such as tracking IP type II bursts [Reiner et al., 2001] and interplanetary scintillation (IPS) [see, e.g., Tokumaru et al., 2000] can provide information on CMEs in the IP medium. However, a number of questions still remain in relating the observed disturbances at radio wavelengths to the white-light CMEs.

By combining near-Sun and near-Earth manifestations of a large number of CMEs, we quantified the influence of the interplanetary medium on CMEs and developed an empirical arrival model to predict the arrival of CMEs at 1 AU [Gopalswamy et al., 2000b, hereinafter paper 1]. This model was based on a set of Earth-directed CMEs observed by the Solar and Heliospheric Observatory (SOHO) that had 1 AU counterparts detected in situ

by the Wind Spacecraft. One of the major limitations of this model is that the remotely measured speeds of CMEs are subject to projection effects. In this paper, we have attempted to remove the projection effects using a set of published archival data [Sheeley et al., 1985; Lindsay et al., 1999] with minimal projection effects.

We do appreciate that predicting the 1-AU arrival of CMEs is only the first step in space weather prediction, because not all CMEs that arrive at 1 AU produce severe geomagnetic storms. It is well known that CMEs must contain a southward magnetic field component in order to cause a geomagnetic storm. Thus, to assess the geoeffectiveness of a CME, we need to consider factors such as CME speed, magnetic field structure, and its ability to drive interplanetary shock.

2. Outline of the Empirical CME Arrival Model

The model developed in paper 1, was based on the fact that the distribution of speeds of interplanetary CMEs (ICMEs) was much narrower than that of the CMEs observed near the Sun. We postulated that CMEs, after their origin at the Sun, interact with the solar wind during their propagation through the IP medium so that they arrive at 1 AU with a different speed. An implicit assumption is that the spatial structure of a CME observed near the Sun is preserved as it propagates through the IP medium to produce the temporal structure observed in situ. For example, the ordering of substructures near the Sun (shock, frontal structure, cavity and prominence core) and at 1 AU (shock, sheath, IP ejecta and pressure pulse) may be preserved at least in some cases (see Table 1 and Gopalswamy et al., [1998b]). The steps involved in the model

are: (i) determine the acceleration for a set of CME-ICME pairs (assuming the CME speed to be the initial speed and ICME speed to be the final speed), (ii) obtain an empirical relation between the acceleration and the initial speed of CMEs, and (iii) obtain travel time from CME onset near the Sun.

The CME speed (u) measured by SOHO's Large angle and spectrometric coronagraph (LASCO) near the Sun ($\sim 2\ R_s$) is related to the ICME speed (v) measured at 1 AU by Wind:

$$v = u + at \qquad (1)$$

where t is the transit time measured as the difference between CME onset and ICME onset and a is the effective interplanetary acceleration. When a (m s^{-2}) is plotted against u (km s^{-1}), the following linear relation was found in paper 1:

$$a = 1.41 - 0.0035u \qquad (2)$$

Assuming that the acceleration behaves in a similar fashion for any new CME, one can obtain the travel time t from the kinematic equation,

$$S = ut + \frac{1}{2}at^2 \qquad (S \sim 1\ \text{AU}) \qquad (3)$$

According to this equation, for speeds in the range 50-1500 km s^{-1}, the 1-AU travel time of CMEs ranges from 1.5 to 5.25 days. This model provides a simple means of advance warning of solar disturbances arriving in the vicinity of Earth. Of course, we need the background information such as disk signatures to confirm that the halo CMEs are frontside events and their location to be close to the central meridian. The initial speed of the CME needs to be measured accurately to get an accurate arrival time.

This simple model has several shortcomings: (i) The measured initial speeds are lower limits to the true speeds due to projection effects. The projection effects depend on the solar surface location of the CME and its width [see, e. g., Sheeley et al., 1999; Gopalswamy et al., 2000c; Leblanc and Dulk, 2001]. (ii) The background solar wind is variable, resulting in different magnitudes of the drag force at different heliocentric distances. A similar effect applies when CMEs are expelled in quick succession from the same region. In this case the slower CME may be cannibalized or deflected and hence the prediction becomes complicated [Gopalswamy et al., 2001]. (iii) CMEs may be accelerating, moving with constant speed or decelerating in coronal images covering a heliocentric distance of $\sim 30\ R_s$). This means the constant acceleration we assumed may not hold. Moreover, the magnitude of the mean acceleration is typically less than that measured in the coronagraphic field of view [Sheeley et al., 1999]. (iv) Once the low-speed CMEs attain the speed of the solar wind, they may move with constant speed thereafter. Thus, assuming a constant acceleration all the way to 1 AU will result in an overestimate of the final speed of slow CMEs. (v) Since CMEs are launched at different initial speeds, the effective acceleration of different CMEs might cease at different heliocentric distances.

Among the above limitations two are particularly serious: the projection effects and the acceleration distance. In this paper, we concentrate on these two issues. CMEs used in the initial study were all Earth-directed (see paper 1), so we measured only the sky-plane speed (the speed with which the CME spreads in the sky plane). This may or may not be the true speed of the CME. Gopalswamy et al. [2000c] found a definite correlation between the sky plane speeds and the corresponding central meridian distance

of the solar source, with the fastest events originating closest to the limb. In order to overcome the projection effects, one needs to have stereoscopic observations. Although there are no such observation at present, some archival observations of CMEs were obtained in quadrature (in situ and remote-sensing spacecraft had orthogonal viewpoints to the Sun), and hence projection effects were minimal. We use these archival data to validate the CME arrival model.

3. Validation of the Model

To eliminate the projection effects we need to measure the nose speed of the CME near the Sun as well as at distances far away from the Sun.   This is possible when a spacecraft along the Sun-Earth line observes a limb CME while another located above the same limb at a distance equivalent to the Sun-Earth distance detects the CME *in situ*. Such an arrangement of spacecraft was available for a few intervals in the past. Helios 1 spent considerable amount of time above both limbs of the Sun, in the ecliptic plane at distances ranging from $\sim$ 0.3 to 1 AU during 1979 to 1982. The Solwind coronagraph on board the P78-1 satellite (located along the Sun-Earth line) remotely imaged CMEs during this period.   Figure 1 shows a typical example of CME observations in quadrature. This is a Solwind image of the 1979 July 3 CME, obtained from the Sun-Earth line. The CME speed is measured by tracking the leading edge (nose) of the CME. The Helios 1 spacecraft was located above the west limb of the Sun at a heliocentric distance of $\sim$ 0.7 AU. The CME arrived at Helios 1 on July 5, 1979 at 15:00 UT. Note that Helios 1 detects roughly the same section of the CME as was done by Solwind two days earlier. Thus, a limb CME for Solwind is a 'halo CME' for Helios 1 whenever Helios 1 is above one of the limbs. It must, however, be pointed out that the in situ spacecraft intersects at only one point, which may not be the nose of the CME. Although the remote-sensing spacecraft reveals the shape of the CME in the sky plane, the in situ spacecraft does not. The relation between the (remote-sensed) CME leading edge and its nose (at the in situ location) depends on the shape of the CME as well as its coordinates (latitude and longitude) relative to the in situ spacecraft. In spite of these difficulties, measurements made from orthogonal viewpoints minimize the projection effects.

Although Helios 1 was not in the vicinity of Earth, it was possible to choose events for which Helios 1 was at a distance of $\sim$ 0.7 AU, similar to the Sun-Earth distance. Sheeley et al. [1985] reported a large number ICMEs that followed IP shocks and were associated with limb CMEs observed by Solwind. Lindsay et al. [1999] expanded Sheeley et al.'s list by including data from Pioneer Venus Orbiter (PVO) which was in quadrature with either P78-1 or the Solar Maximum Mission (SMM). The Coronagraph/Polarimeter on board SMM imaged CMEs in the 1980s. We revised the list of Lindsay et al. [1999] eliminating uncertain events and came up with a set of 19 CME-ICME pairs (see Table 1) observed by the Solwind coronagraph (remotely) and by PVO or Helios-1 (locally). In order to be consistent with our analysis, we did not include events for which the local-sensing spacecraft was at distances $<$ 0.6 AU. We also excluded the SMM events because the SMM measurements correspond to the cavity of the CMEs [Burkepile and St. Cyr, 1993], rather than the frontal structure. In columns 2-7 of Table 1, we list the onset date, day of the year, universal time, *in situ* speed, heliocen-

tric distance of the spacecraft and the measuring spacecraft. In columns 8-11, we provide information on the corresponding white-light CMEs: the CME onset date, universal time, speed, and position angle. The measured transit time (difference between CME and ICME onsets) is listed in column 12. The local-sensing spacecraft were located at heliocentric distances ranging from 0.63 AU to 0.91 AU, but most were around 0.72 AU. The sky plane speeds are probably closer to the actual speed because for events originating typically within 30° of the limb, the angular scattering function differs from the limb value only by 3.4% [see, e.g., Bird and Edenhofer, 1990].

We repeated the analysis as in the case of SOHO/Wind events in paper 1: the effective acceleration was obtained by dividing the difference between the CME and ICME speeds by the transit time to the local-sensing spacecraft. The resulting empirical relation between the effective acceleration (a) and initial speed (u) maintained the same functional form as in paper 1:

$$a = 2.193 - 0.0054u, \qquad (4)$$

with a slight change in the coefficients. The solid line in Figure 2 represents the above equation (the data points are marked by the "plus" symbols). The dashed line represents equation (2). The major difference between the SOHO/Wind and P78-1/PVO-Helios acceleration models is that the latter has a slightly steeper slope. This is consistent with the removal of projection effects: in paper 1, we underestimated the CME initial speed resulting in an overestimate of the acceleration. A quadratic fit to the P78-1/PVO-Helios data points, shown by the dotted line in Fig. 2, is very close to the linear fit. The quadratic fit may have implications to the physics of CME interaction with the solar wind: near the Sun,

the coronal drag depends on the square of the CME speed for low solar wind speeds [see, e.g., Chen, 1997 and references therein].

3.1. The New Prediction Curve

The next step is to use the derived acceleration model (eq. 4) in equation (3), to get the new prediction curve. Note that this acceleration model was obtained from ICME speeds measured at different heliocentric distances (see, Table 1) with a mean value of ~ 0.76 AU. If we assume that the mean acceleration is constant, we can use this acceleration model as was done in paper 1. However, as we discussed before, the acceleration might end at some distance less than 1 AU. In the following we assess the influence of relaxing the assumption of constant acceleration.

If the CME starts out with a speed u, it will have a speed v at a distance S according to the the kinematic equation,

$$v^2 = u^2 + 2aS. \qquad (5)$$

We see that for $a < 0$, the final speed could be zero when $u^2 = 2|a|S$, which is not possible because the final speed asymptotically reaches the solar wind speed. For CMEs starting out faster than the solar wind, the deceleration must stop when $u^2 - 2|a|S = v_{sw}^2$. Similarly, for CMEs starting out slower than the solar wind, the acceleration must stop when $u^2 + 2aS = v_{sw}^2$. Assuming the solar wind speed to be 400 km s^{-1}, we can estimate the distance at which a CME would approach the solar wind speed. This distance is plotted in Fig. 3 which shows that the slow CMEs must cease to accelerate around 0.2 AU while the fast events stop decelerating at larger distances. For higher solar wind speeds, this distance will increase for slow CMEs and decrease for fast CMEs. It is a happy coincidence that the PVO-Helios measurements

were made at heliocentric distances similar to the ones in Fig. 3. Therefore, we assume that the final speeds measured by PVO-Helios change little after the CMEs propagate past the spacecraft.

To generalize the above argument, we assume that the effective acceleration ceases at some distance (d_1) from the Sun and the CMEs travel with a constant speed beyond d_1 to reach a point near Earth at a distance d_2 from d_1. We refer to d_1 as the "acceleration-cessation" distance or simply the acceleration distance. The travel time, then, is the sum of the time (t_1) taken to travel the distances d_1,

$$t_1 = \frac{-u + \sqrt{u^2 + 2ad_1}}{a}, \qquad (6)$$

and that (t_2) to travel d2:

$$t_2 = \frac{d_2}{\sqrt{u^2 + 2ad_1}}. \qquad (7)$$

Substituting for a from equation (4), we calculate the total travel time $t = t_1 + t_2$ from the above equations. This is predicted 1-AU arrival time of the CMEs.

In Figure 4 we have shown the total travel time ($t_1 + t_2$) for various values of d_1: (A) 0.76, (B) 0.85, and (C) 0.95 AU with $d_2 = 1 - d_1$. The first segment t_1 of the travel time is shown for various values of d_1 in dashed lines. For one case, ($d_1 = 0.76$ AU and $d_2 = 0.24$ AU), we have also shown t_2 (dotted line). The total travel time $t_1 + t_2$ for this case is the solid curve "A". It is clear that the effect of cessation of acceleration is to make the travel time of low speed CMEs to be roughly constant, irrespective of their initial speed.

3.2. Comparison Between Prediction Curves

The quadratic fit to the acceleration-speed plot (see, Fig. 2) can also be used in the kinematic equation to obtain prediction curves.

These curves are represented by the three dashed lines in Fig. 5 corresponding to d_1 = 0.76, 0.85, and 0.95 AU. The solid curves (A, B, and C), derived from the P78-1/PVO-Helios data correspond to the three acceleration-cessation distances (0.76, 0.85 and 0.95 AU, see Fig. 4). The curves based on the quadratic acceleration model are similar to the ones based on the linear acceleration model for high speed CMEs. The two sets of curves disagree considerably for most other speeds. For comparison, we have also shown the zero acceleration case (dotted line), which assumes that the CME and ICME have the same speed (unrealistic case). The prediction curve from paper 1 is shown by the dot-dashed line. We have also included the constant 1-AU arrival time of 80 hours (thin horizontal line) obtained by Brueckner et al. [1998]. The observed, roughly flat arrival times for low speed CMEs is best represented by the curves A, B, C (linear acceleration cases), and they are not too different from the quadratic cases at high initial speeds. Therefore, we regard the prediction curves with linear acceleration model as improved compared to the curve obtained in paper 1. In the next section, we test the prediction curves using new observations of SOHO/Wind CME-ICME pairs.

4. Testing with New Data

We selected 47 of the recent ICME events with clear ejecta (EJ) or magnetic cloud (MC) signatures in the in situ magnetic field - plasma measurements. MCs are structures that follow the sheaths of the IP shocks with high magnetic field, smooth rotation of the field and low proton temperature [see, e.g. Burlaga, 1988]. In the case of ejecta, smooth rotation may not be present. We refer to MCs and EJs collectively as ICMEs. In Table 2 we have listed the 47 events, including the 23 events

from paper 1. The remaining 24 events correspond to the period October 1998 to July 2000. We used Wind data to gather information on these events. Whenever the Wind spacecraft was not in the solar wind, we used data from ACE. As before, we were able to identify a unique white-light CME for each of these IP events. Since our purpose is to evaluate the prediction capability of our model, we did not make the list exhaustive. For example, a larger number of ejecta has been reported by Lepri et al., [2001] based on Fe compositional signatures. Improper identification of ICMEs can result in incorrect conclusions: Cane et al. [2000] identified a set of ICMEs, primarily based on cosmic ray depression. Since cosmic ray depression starts behind IP shocks and ahead of ICMEs [see, e.g., Burlaga, 1991], their identification corresponds to the onset of IP shocks rather than the ICMEs that follow the shocks by 0.5 day. This led to their incorrect conclusion that the ejecta in their study arrived earlier than our prediction in paper 1. In view of this, we confine to those ICMEs identified using magnetic signatures described above. In columns 2 to 6 of Table 2, we have listed the day of year, date, approximate onset time, the X component of the speed in GSE coordinates and internal structure (MC or EJ), respectively. In paper 1 we had used the total speed for the ICMEs. In most of the cases, the X-component was very close to the total speed. MC? represents an event with low confidence level for the structure to be an MC but high confidence level to be an EJ. Ejecta structures with low confidence level are marked as EJ?. In columns 7 to 11, we have listed the CME data from SOHO/LASCO observations: date, time, type, location of eruption on the disk and speed, respectively. The CME speed used here is the speed of the fastest feature within the LASCO field of view. The measured travel time (difference between CME and ICME onsets) is listed in column 12.

The measured travel times in column 12 of Table 2 are plotted on the prediction curve (see Fig. 6a). We have used the prediction curves corresponding to the acceleration distance of 0.76 and 0.95 AU. Given the uncertainties in the acceleration the agreement between the model and the data is rather good. The distribution of travel times for slow CMEs is consistent with the flat profile of the prediction curve. However, the slow CMEs seem to arrive slightly ahead of the prediction. This means that the slow CMEs must be accelerating to speeds faster than the solar wind speed much before 0.76 AU. This is also consistent with the larger measured acceleration within the coronagraphic field of view [Sheeley et al., 1999] than the average values indicated by equation (4).

4.1. Projection Effects

In Fig. 6a, the CME speeds were obtained in the plane of the sky using LASCO coronagraph data. As we stated in paper 1, the space speed of CMEs may be larger than the sky plane speed because of projection effects. Based on an earlier work by Sheeley et al. [1999], Leblanc and Dulk [2001] attempted to correct the measured sky plane speed using the known latitude (ψ) and longitude (λ) of the eruption region using the relation,

$$u_r = u_s \frac{(1 + sin\phi)}{(sin\phi + sin\alpha)} \qquad (8)$$

where u_r and u_s are the space and sky-plane speeds, respectively. α is the cone angle of the CME (half width) and ϕ is obtained from the longitude and latitude of the eruption region:

$$cos\phi = \cos \lambda cos\psi. \qquad (9)$$

The major uncertainty in the equation for u_r is the cone angle of the CME, which is impossible to measure for halo CMEs we are dealing with. Recently, Dasso et al. [2001, under preparation] investigated the effect of cone angle on the projection correction and found that the correction factor lies in the range 2 to 7 for cone angles in the range $10° - 60°$ for a CME originating from the disk center. It is well known that limb CMEs have a range of widths, so there is no simple way to assign widths to different CMEs. One possibility is to use the average width (cone angle = $36°$, see St Cyr et al., [2000]) as was done by Leblanc and Dulk [2001]. For this case, the correction factor ranges from ~ 2.5 for disk-center events to ~ 1.5 for events originating at a longitude of $40°$. Another major uncertainty arises from the fact that the latitude ψ obtained from the solar source may not accurately represent that of the white-light CME because of the early nonradial motions [Gopalswamy et al., 2000a].

With these caveats, we assumed a cone angle of $36°$ and applied the correction factor to the measured initial speeds. The correction extended the range of initial speeds to ~ 2700 km s^{-1}. The corrected speeds were used in Fig. 6b to compare the measured and predicted travel times. It is obvious from Fig. 6b that the agreement between measured and predicted travel times worsened. In fact, the agreement was much better when uncorrected initial speeds were used (see Fig. 6a). This suggests that we overcorrected for many events.

Since the new prediction model is based on data with minimal projection effects, one would have expected a better agreement between predicted and measured travel times after projection correction. In estimating the projection correction, we assumed that the CME is a rigid cone and assumed that the sky-plane speed is precisely the actual speed projected on the sky plane. However, when the CME expands in addition to radial motion, the measured sky-plane speed is a sum of the expansion speed and the projected radial speed. If the CME is expanding rapidly in the beginning, the space speed may be comparable to the sky-plane speed. The good agreement between the predicted and measured travel times without projection correction suggests that the projection effects are somehow compensated for by the initial expansion of the CME. This also would imply that the CME may not be a rigid cone as often assumed. Since there is no simple way to obtain the widths of halo CMEs, the sky-plane speed seems to be a reasonable representation of the CME initial speed.

4.2. Estimated Error

Figure 7 shows the computed error in the arrival time for the prediction curves in paper 1 (based on SOHO/Wind data) and in this work (P78-1/PVO-Helios 1 data). The error is defined as the deviation from the prediction curve for each of the measured travel times in Table 2. We use the prediction curve corresponding to an acceleration-cessation distance of 0.76 AU (curve A in Fig. 5) since it represents the observations quite well. For the prediction curve of paper 1, the error has a flat distribution with a peak around 6 hrs. For the new curve, the error has a gaussian distribution with a peak at -6 hours. The mean error of 10.7 hours for the new model is $\sim 50\%$ lower than the error (15.4 hours) computed using the previous model. Clearly, the average error decreased considerably when we used the P78-1/PVO-Helios acceleration model. From the histogram we note that 72% of the events have arrival times within ± 15

hours from the predicted values. In Figure 8, where we have plotted the observed and predicted transit times for the 47 events with the two dashed curves marking a deviation of 18 hours from the prediction curve. For CME speeds ≥ 400 km s^{-1}, only one point is outside the dashed curves. For slower CMEs, there are 6 points outside the region bounded by the dashed curves. The assumption of constant acceleration and the variability in the background solar wind might be responsible for the scatter of the data points around the prediction curve. In fact different CMEs are likely to stop accelerating at different distances based on their initial speed and the speed of the solar wind. Note that our model is based on observable parameters such as the CME initial speed; it does not incorporate the variability of solar wind speed explicitly because one cannot measure it near the Sun (on-disk).

5. Discussion and Conclusions

We have validated the empirical CME arrival model of Gopalswamy et al. [2000b] using a set of CME-ICME observations obtained by P78-1, Helios-1 and PVO missions as reported in Sheeley et al. [1985] and Lindsay et al. [1999]. We used only a subset of events listed by these authors that had measurements at distances > 0.6 AU. We obtained a new prediction curve, which is significantly better than the previous one. The two primary changes we made are: 1. obtaining an interplanetary acceleration using data with minimal projection effects, and 2. incorporating the possibility of cessation of the interplanetary acceleration somewhere between the Sun and 1 AU. The prediction curve based on the new acceleration model yields arrival times ∼ a day shorter than the original model for low speed CMEs. The difference between

the two prediction curves is not significant for high speed CMEs. The error in the arrival times is also significantly smaller when the new acceleration model is used.

We now compare our prediction results with those of a parametric study of magnetic cloud propagation by Vandas et al. [1996]. Their inner boundary started at 18 R_s, so their travel time may be off by a few hours corresponding to the travel from the solar surface to 1 AU. For slow (250 km s^{-1}) and fast (750 km s^{-1}) background solar wind, they obtained travel time (in hours) as $t = 85 - .014u$ and $t = 42 - 0.004u$, respectively. Here u is the initial speed (in km s^{-1}) of the magnetic cloud at 18 R_s. These lines intersect our prediction curve for $u = 875$ km s^{-1} (slow-wind), and $u = 1500$ km s^{-1} (fast-wind) but deviate enormously from our model as well as observations at other locations. In fact most of the data points lie above both slow- and fast-wind models of Vandas et al. [1996]. To compare specific cases, let us consider an initial speed of 500 km s^{-1} (lowest speed used in the simulation of Vandas et al.), almost all the CMEs arrived according to our prediction (∼ 4.3 days), while the slow- and fast-wind models predict 3.25 and 1.67 days, respectively. On the high-speed side, we have the Bastille day CME (event #45 in Table 2) to compare. It started out with an initial speed of ∼ 1674 km s^{-1} and arrived at 1 AU after 35.1 hours. Our model predicts a travel time of ∼ 31.2 hours, while the slow- and fast-wind models predict 61.6 and 35.3 hours, respectively. In other words, our prediction is only 11% away from the observed travel time, while the prediction of the slow-wind model is off by ∼ 76%. The close agreement of the fast-wind model with the observation is fortuitous because the fast-wind curve intersects our model around this initial speed. Moreover, there is

no a priori reason to assume that the Bastille day CME was ejected into a 750 km s^{-1} solar wind at 18 R_s. In fact, the 1-AU speed of the solar wind at the time of the white-light CME was in the range 550-600 km s^{-1}. If we extrapolate their fast-wind model to a background speed of 600 km s^{-1}, we get $t = 55 - 0.006u$, which yields $t = 45$ hours, compared to the observed 35.1 hours. Thus, we conclude that our model better represents the observed travel time for the events in the study period.

One of the surprising results of this study is that the prediction of 1-AU arrival times of CMEs based on their initial sky-plane speed is much better than that with projection correction. This shows that simple projection correction based on the solar-source location of CMEs and an assumed cone angle is not adequate. The projection effects seem to be partly compensated for by the initial expansion of the CME. The results of our attempt to correct for projection effects of SOHO/LASCO CMEs, and the difference between observed and predicted arrival times of slow CMEs suggest that CMEs accelerate and expand inside 0.7 AU to an extent more than our model supposes. Moreover, different CMEs are expected to have different widths, so the use of an average width for all the CMEs may not be justified. This does not mean projection effects are unimportant. In fact, the improved estimate of the IP acceleration is a direct result of minimizing projection effects using quadrature observations. The orthogonal viewpoints of the spacecraft in quadrature directly reduce the projection effects, without involving CME widths.

References

Bird, M. K. and P. Edenhofer, Remote sensing observations of the corona, in *Physics of the Inner Heliosphere, 1. Large-scale Phenomena*, edited by R. Schwenn and E. Marsch, Springer-Verlag, New York, p. 13, 1990.

Bravo, S. and X. Blanco-Cano, Signature of interplanetary transients behind shocks and their associated near-surface activity, Ann. Geophysicae, 16, 359, 1998.

Brueckner, G.E., et al., Geomagnetic storms caused by coronal mass ejections (CMEs): March 1996 through June 1997, *Geophys. Res. Lett., 25*, 3019, 1998.

Burkepile, J. and O. C. St. Cyr, A revised and expanded catalogue of mass ejections observed by the Solar Maximum Mission coronagraph, National Center for Atmospheric Research, Boulder, CO, 1993.

Burlaga, L. F., Magnetic Clouds: Constant alpha force-free configurations, *J. Geophys. Res., 93*, 7217, 1988.

Burlaga, L. F., Magnetic Clouds, in *Physics of the Inner Heliosphere, 2. Particles, Waves and Turbulence*, edited by R. Schwenn and E. Marsch, Springer-Verlag, New York, p. 11, 1991.

Burlaga, L., R. Fitzenreitter, R. Lepping, K. Ogilvie, A. Szabo, A. Lazarus, J. Steinberg, G. Gloeckler, R. Howard, D. Michels, C. Farrugia, R. P. Lin, and D. E. Larson, A magnetic cloud containing prominence material: January 1997, *J. Geophys. Res., 103*, 277, 1998.

Cane, H, V., The relationship between coronal transients, Type II bursts and interplanetary shocks, *Astron. Astrophys., 140*, 205, 1984.

Cane, H, V., I. G. Richardson, and O. C. St. Cyr, Coronal mass ejections, interplanetary ejecta and geomagnetic storms, *Geophys. Res. Lett., 27*, 3591, 2000.

Chen, J., Coronal mass ejections: causes and consequences, A theoretical view, in *Coronal Mass Ejections*, edited by N. Crooker, J. A. Joselyn, and J. Feynman, (Geophys. Monogr. 99; Washington DC: AGU), p. 65, 1997.

Gopalswamy, N. et al., On the relationship between coronal mass ejections and magnetic clouds, *Geophys. Res. Lett., 25*, 2485, 1998a.

Gopalswamy, N., M. L. Kaiser, R. P. Lepping, S. W. Kahler, K. Ogilvie, D. Berdichevsky, T. Kondo, T. Isobe and M. Akioka, Origin of Coronal and Interplanetary Shocks: A new Look with WIND Spacecraft Data, *J. Geophys. Res., 103*, 307, 1998b.

Gopalswamy, N., Y. Hanaoka, and H. S. Hudson, Structure and dynamics of the corona surrounding an eruptive prominence, *Adv. Space Res., 25 (9)*, 1851, 2000a.

Gopalswamy, N., Lara, A., Lepping, R. P., Kaiser, M. L., Berdichevsky, D., St. Cyr, O. C., Interplanetary acceleration of coronal mass ejections, Geophys. Res. Lett. Vol. 27 , No. 2 , p. 145, 2000b (paper 1).

Gopalswamy, N., M. L. Kaiser, B. J. Thompson, L. F. Burlaga, A. Szabo, A. Vourlidas, A. Lara, S. Yashiro, and J.-L. Bougeret, Radio-rich Solar Eruptive Events, *Geophys. Res. Lett., 27*,1427, 2000c

Gopalswamy, N., S. Yashiro, M. L. Kaiser, R. A. Howard, and J.-L. Bougeret, Radio signatures of coronal mass ejection interaction: Coronal mass ejection cannibalism?, *Astrophys. J., 548*, L91, 2001.

Gosling, J. T., The solar flare myth, *J. Geophys. Res., 98*, 18937, (1993).

Haurwitz, M. W., S. Yoshida, and S.-I. Akasofu, Interplanetary magnetic field asymmetries and their effects on polar cap absorption events and Forbush decreases, *J. Geophys. Res., 70*, 2977, 1965.

Howard, R. A., D. J. Michels, N. R. Sheeley and M. J. Koomen, The observations of a coronal transient directed at Earth, *Astrophys. J., 263*, L101, 1982.

Lara, A. et al., Interplanetary Acceleration of Coronal Mass Ejections; A Numerical Test, *J. Geophys. Res.*, under preparation, 2001.

Leblanc, Y., and G. A. Dulk, Tracing shock waves from the corona to 1 AU: Type II radio emission and relationship with CMEs, *J. Geophys. Res.*, in press, 2001.

Lepri, S. T., T. Zurbuchen, L. A. Fisk, I. C. Richardson, H. V. Cane, and G. Gloeckler, Ion charge distribution as an identifier of coronal mass ejections, *J. Geophys. Res.*, in press, 2001.

Lindsay, G. M., J. G. Luhmann, C. T. Russell, and J. T. Gosling, Relationship between coronal mass ejection speeds from coronagraph images and interplanetary characteristics of associated interplanetary coronal mass ejections, *J. Geophys. Res., 104*, 12515, 1999.

Michels, D. J., R. A. Howard, M. J. Koomen, S. Plunkett, G. E. Brueckner, P. Lamy, R. Schwenn, and D. A. Biesecker, Visibility of Earth-directed Coronal Mass Ejections, in Proc. of Fifth SOHO Workshop, ESA SP 404, p. 567, 1997

Reiner, M. J., M. L. Kaiser, N. Gopalswamy, H. Aurass, G, Mann, A. Vourlidas, and M. Maksimovic, Statistical analysis of coronal shock dynamics implied by radio and white-light observations, *J. Geophys. Res.*, in press, 2001.

Sheeley, Jr., N. R., et al., Coronal mass ejections and IP shocks, *J. Geophys. Res., 90*, 163, 1985.

Sheeley, Jr., N. R., J. H. Walters, Y.-M. Wang, and R. A. Howard, Continuous tracking of coronal outflows: Two kinds of coronal mass ejections, *J. Geophys. Res., 104*, 24739, 1999.

St. Cyr, O. C., et al., Properties of coronal mass ejections: SOHO LASCO observations from January 1996 to June 1998, *J. Geophys. Res.,*

105, 18,169, 2000.

Tokumaru, M., M. Kojima, K. Fujiki, and A. Yokobe, Three-dimensional propagation of interplanetary disturbances detected with radio scintillation measurements at 327 MHz, *J. Geophys. Res., 105*, 10,435, 2000.

Vandas, M., S. Fischer, M. Dryer, Z. Smith, and T. Detman, Parametric study of loop-like magnetic cloud propagation, *J. Geophys. Res., 101*, 16,545, 1996.

N. Gopalswamy and S. Yashiro Center for Solar Physics and Space Weather, The Catholic University of America, Washington DC 20064

A. Lara, Instituto de Geofisica, UNAM, Mexico DF, 04510, Mexico.

M. L. Kaiser, Bldg 2, Rm 105, NASA/GSFC, Greenbelt, MD, 20771.

R. A. Howard, Space Sciences Division, Naval Research Laboratory, Washington DC 20375.

[1]Center for Solar Physics and Space Weather, The Catholic University of America, Washington DC.

[2]NASA/GSFC, Greenbelt, MD.

[3]Instituto de Geofisica, UNAM, Mexico DF.

[4]Naval Research Laboratory, Washington DC.
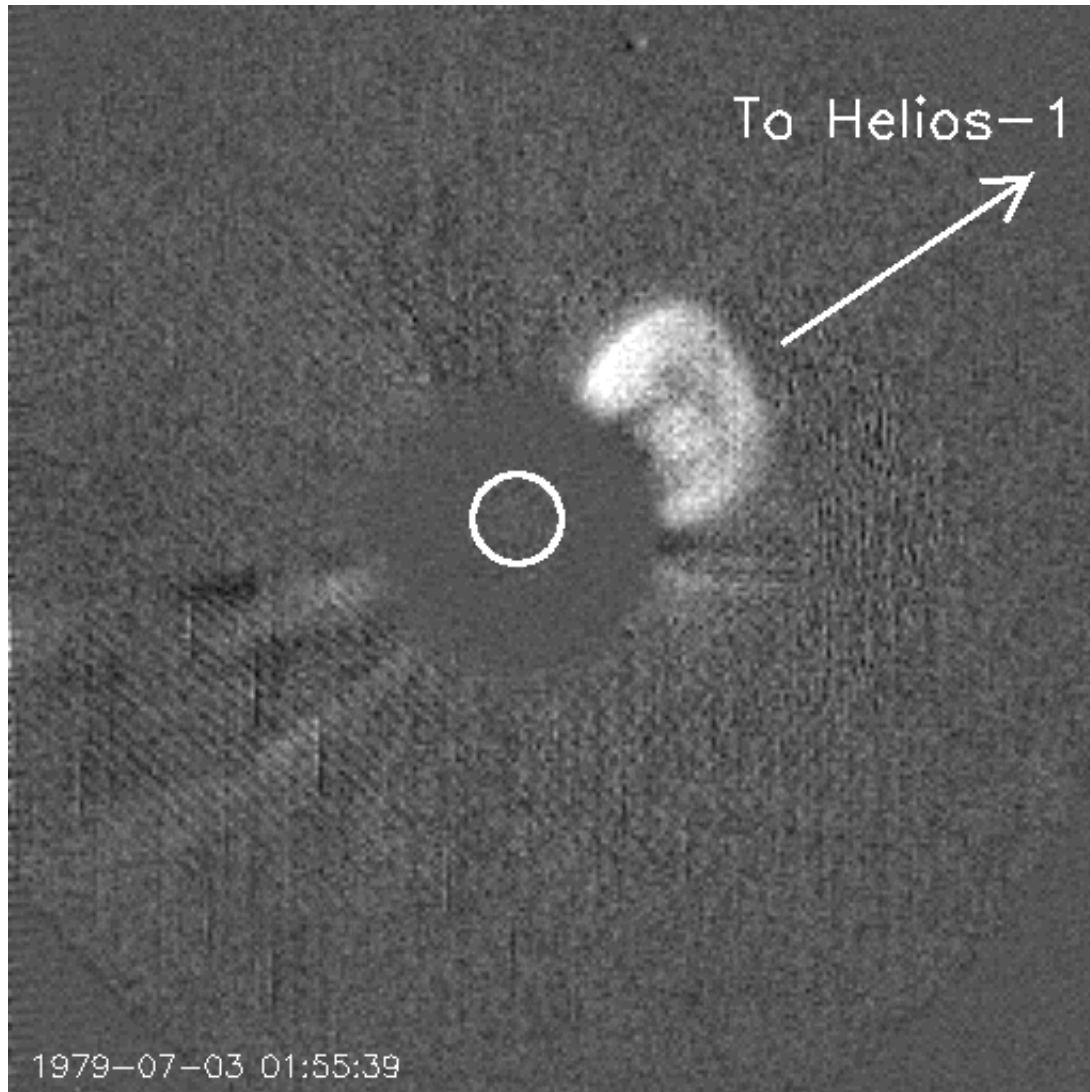
Figure 1. The 1979 July 3 CME observed by the Solwind coronagraph on board the P78-1 satellite is shown heading towards the Helios-1 spacecraft.

Figure 2. The mean acceleration versus initial speed of CMEs obtained from Helios-1/PVO and P78-1 data listed in Table 1. The '+' symbols indicate the data points. The thick solid line and the dotted line are the linear and quadratic fits, respectively to the data points. The dashed line is the acceleration model from paper 1.

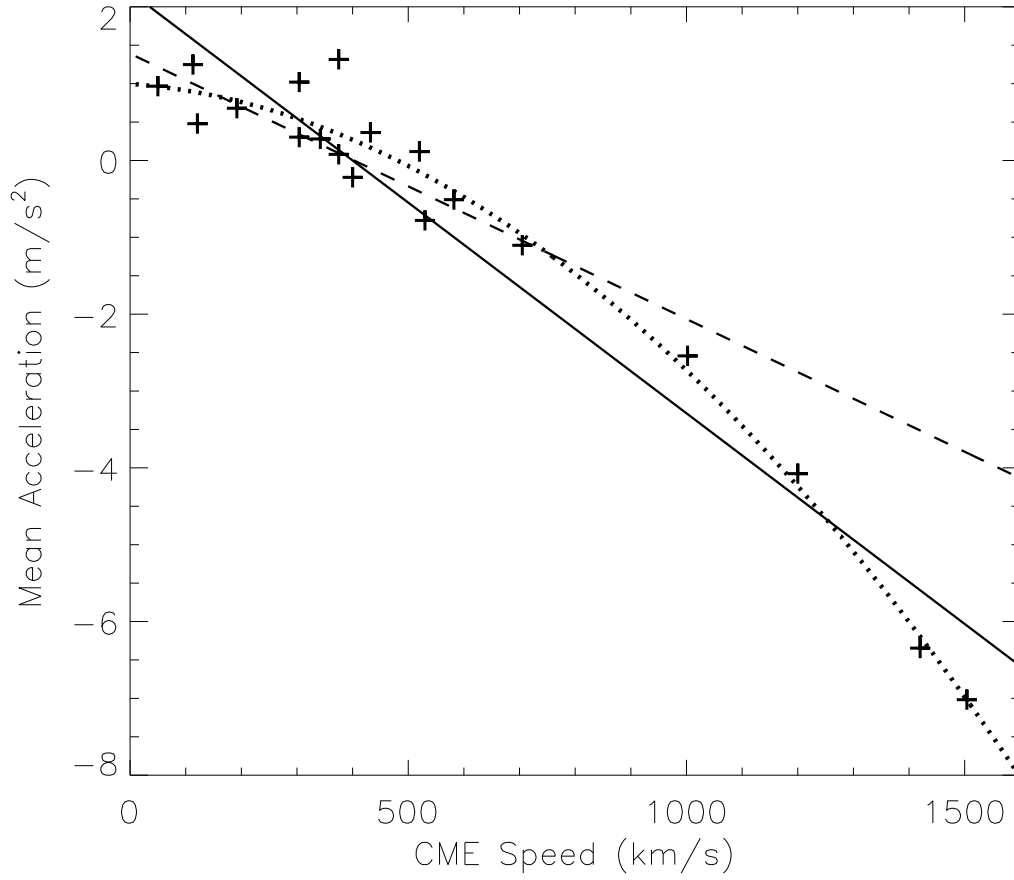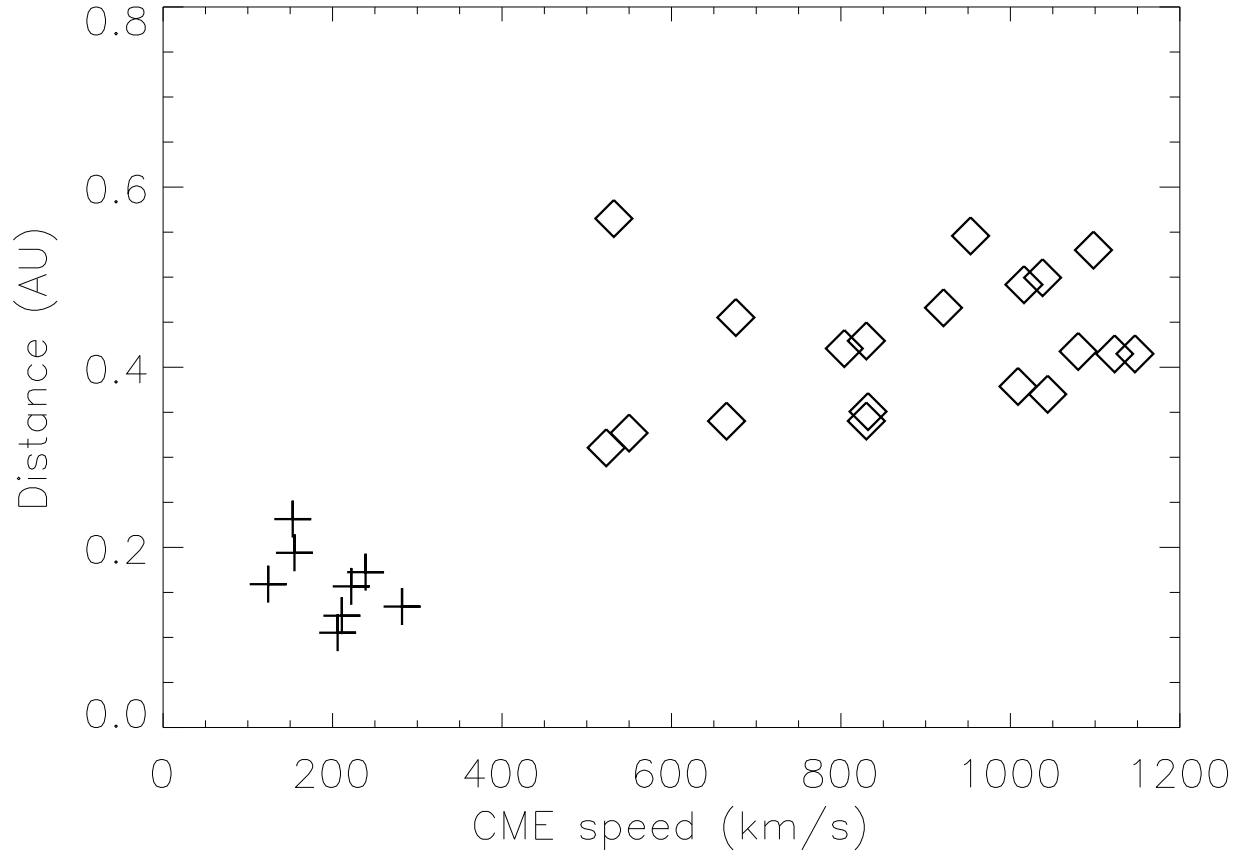**Figure 3.** The acceleration-cessation distance as a function of initial speed of CMEs. The acceleration should go to zero when the ICME speed is approximately equal to the solar wind speed. A solar wind speed of 400 km/s is assumed for this plot. The slow (< 300 km/s) and fast (> 500 km/s) CMEs are represented by '+' and diamonds symbols, respectively. Note that the slow CMEs stop accelerating at much shorter distances.
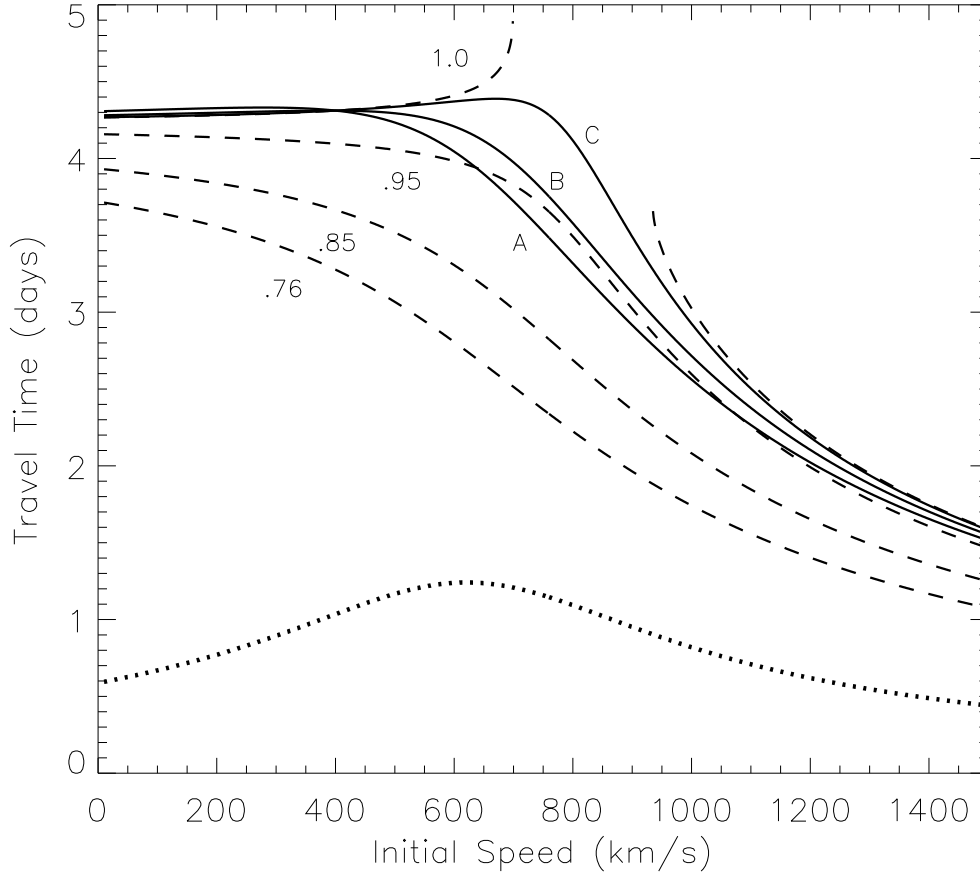
Figure 4. Travel times computed assuming constant acceleration up to different heliocentric distances (0.76, 0.85, 0.95 and 1 AU) are denoted by the dashed lines. Beyond these points, the CME travels with constant speed. The travel time for the zero-acceleration segment for the case in which the acceleration ceases at 0.76 AU is given by the dotted line. The total travel time is the sum of a $\neq$ 0 and a = 0 travel times, as given by the solid curves A, B and C, corresponding to the acceleration-cessation distances 0.76, 0.85 and 0.95 AU, respectively.
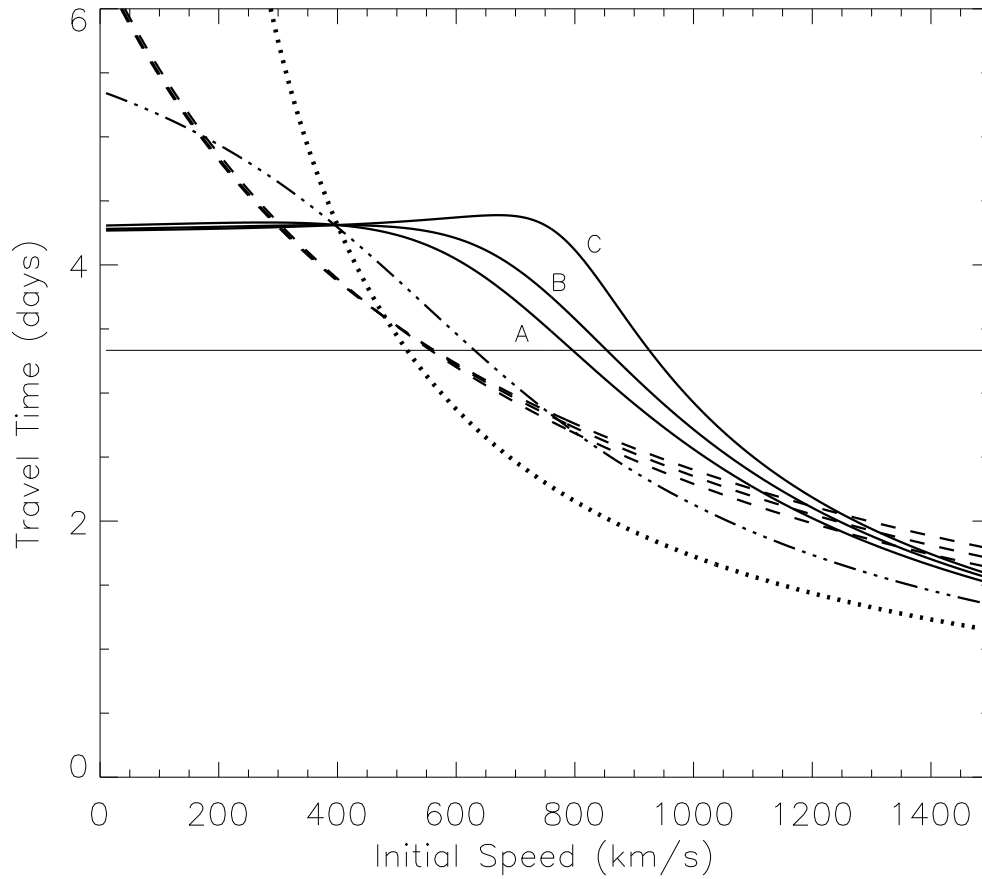
Figure 5. CME arrival models for various cases. The dot-dashed line is from paper 1 based on LASCO/Wind data. All the others are for the acceleration obtained from the P78-1/Helios-1/PVO data. The three solid curves A,B,C correspond to the acceleration cessation distances of 0.76, 0.85, and 0.95 AU, respectively with a linear fit to the acceleration. The dashed curves correspond to the same three cases, except for a second order fit to the acceleration. The horizontal line is the "Brueckners rule."
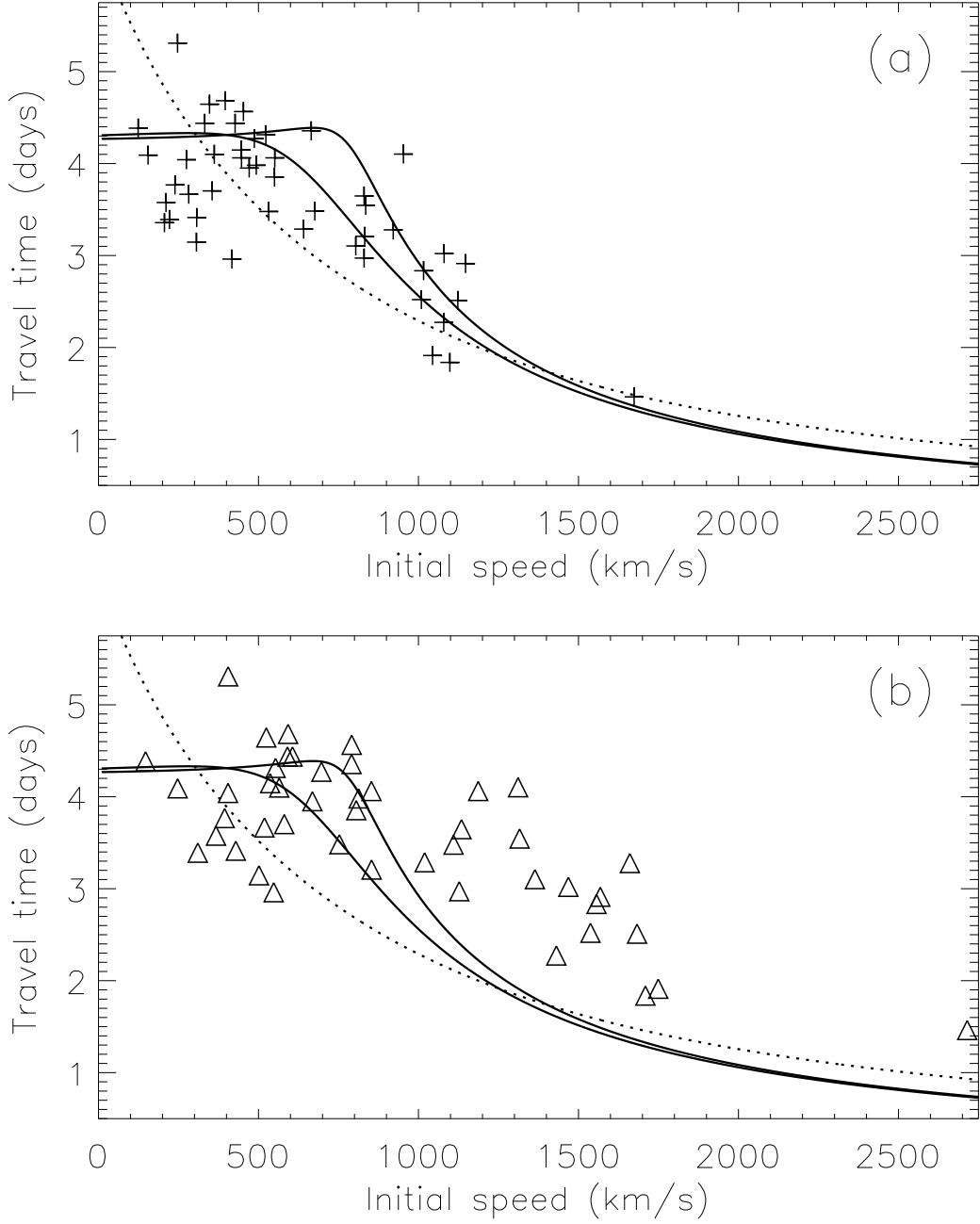
Figure 6. (a) Comparison between predicted and observed travel times based on the acceleration profile obtained in this work. Both linear (solid curves) and quadratic (dotted curve) acceleration cases are shown. The solid curves show the influence of the acceleration-cessation distance (lower – 0.76 AU and upper– 0.95 AU). The plus symbols denote the data points from Table 2. b) same as in (a), but the data points are corrected for projection effects.
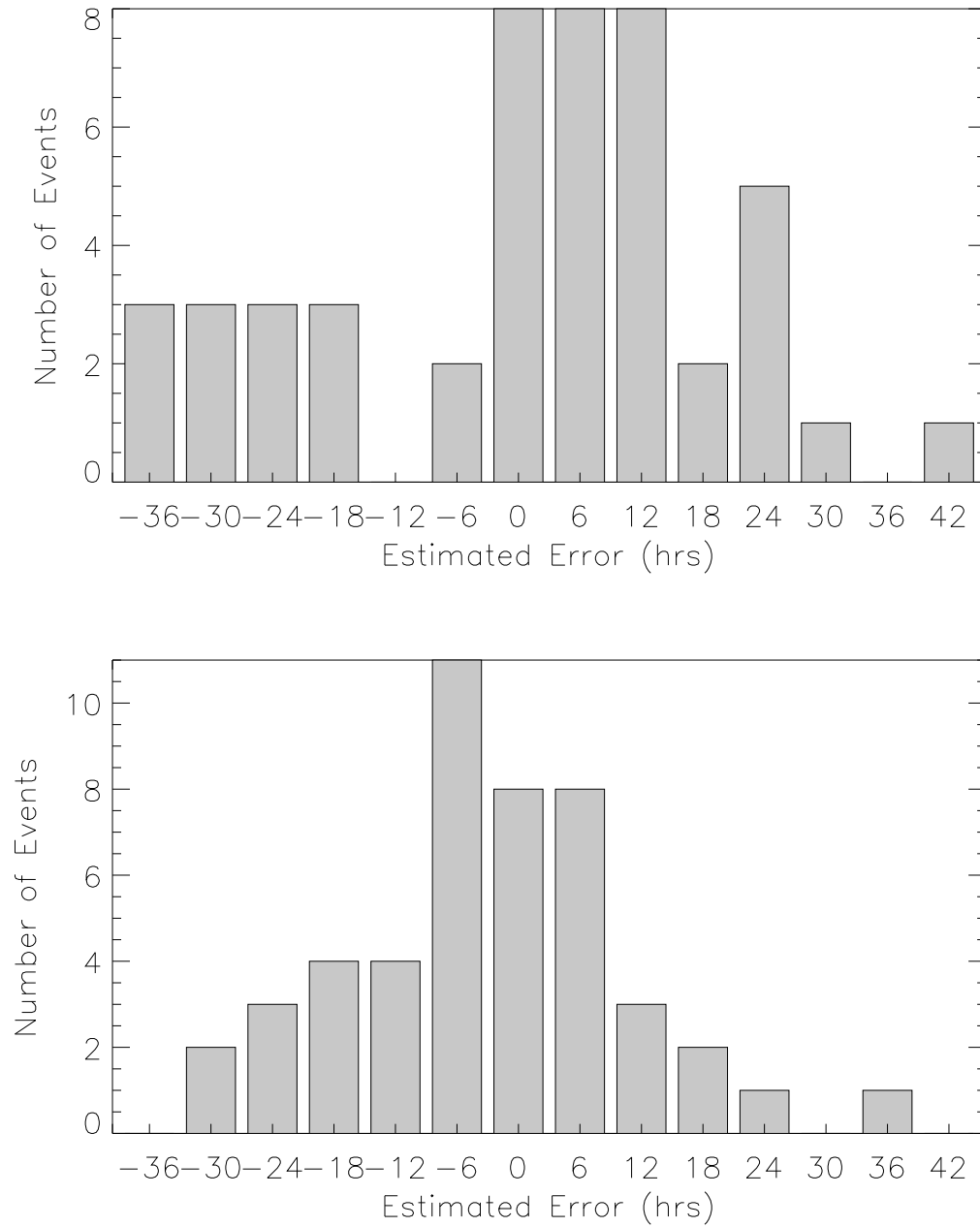
Figure 7. A histogram of the estimated error using the SOHO/Wind (top panel) and the PVO-Helios-1/Solwind (bottom panel) models, the bin size is 6 hrs.

Figure 8. A representative prediction curve of CME arrival time (curve A in Fig. 4) with the +/- 18 hour boundaries given by the dashed lines. The diamonds denote the observed travel times from table 2.

Table 1. CME and ICME Events from P78-1, Helios 1 and PVO

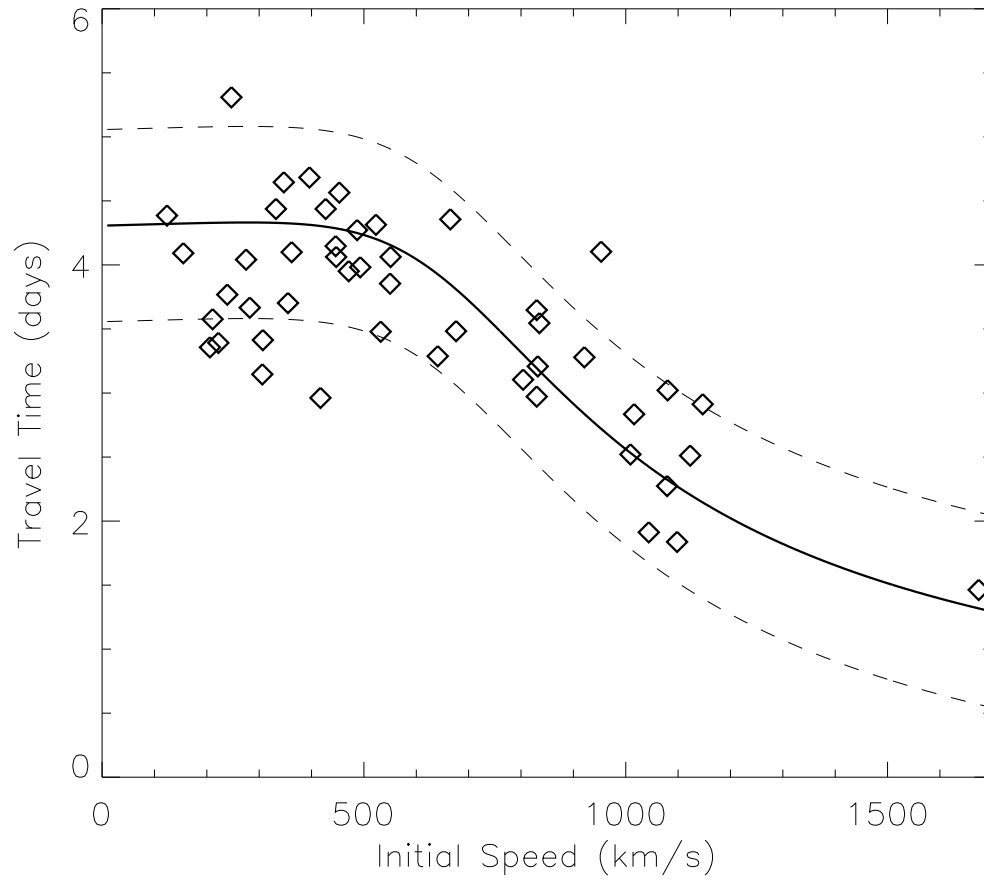| No.	ICME Date	DOY	UT	v^h	Dist	S/C[i]	CME Date	UT	u^j	PA[k]	T.T.
1	May 10, 1979	130	1000	600	0.73	PVO	May 08,1979	1028	375	SW	47
2[a]	July 05,1979	186	1500	470	0.84	He1	July 03, 1979	0156	582	NW	61
3[b]	July 21, 1979	202	2200	362	0.72	PVO	July 19, 1979	1010	530	NW	59
4	March 17, 1980	077	09:00	285	0.72	PVO	March 13, 1980	0955	121	NE	95
5[b]	March 22, 1980	082	1900	399	0.92	He1	March 19, 1980	0706	375	SE	83
6[c]	March 30, 1980	090	0100	560	0.88	He1	March 26, 1980	0047	520	SE	96
7	July 11, 1980	193	1830	541	0.77	He1	July 09, 1980	0158	304	NW	64
8	July 21, 1980	203	1500	338	0.85	He1	July 18, 1980	0842	400	SW	78
9	Aug. 01, 1980	214	1600	409	0.91	He1	July 29, 1980	1331	705	SW	74
10	May 11, 1981	131	1500	818	0.66	He1	May 10, 1981	1239	1420	E	26
11	May 14, 1981	134	1200	702	0.63	He1	May 13, 1981	0415	1504	NE	31
12[d]	July 06, 1981	187	1900	500	0.72	PVO	July 04, 1981	1506	432	SE	51
13	Aug. 23, 1981	235	0600	431	0.72	PVO	Aug. 19, 1981	1346	342	SE	88
14	Oct. 13, 1981	286	2000	650	0.73	PVO	Oct. 12, 1981	0533	1002	SE	38
15[e]	Oct. 28, 1981	301	2000	472	0.73	PVO	Oct. 24, 1981	0217	190	SE	114
16	Aug. 18, 1982	230	0600	413	0.72	PVO	Aug. 14, 1982	0214	304	SW	99
17[f]	May 02, 1983	122	1100	400	0.72	PVO	April 28, 1983	0624	50	N	100
18[b]	Jan. 26, 1984	026	1430	492	0.72	PVO	Jan. 23, 1984	0210	113	W	84
19[g]	Feb. 17, 1984	048	1300	798	0.73	PVO	Feb. 16, 1984	0936	1200	SW	27

The abbreviations are DOY - day of the year; UT - universal time; Dist is the heliocentric distance (AU) of the spacecraft that makes in situ measurements; S/C - observing spacecraft;PA - position angle, and T.T. - travel time in hours.

[a]alternate CME on 07/04 11:38 (speed = 360 km/s).

[b]ICME time is different from Lindsay et al. 1999.

[c]no CME on March 27, 1980 on the East limb. Maybe incorrect identification by Lindsay et al. 1999.

[d]alternate CME on July 04, 1981 at 17:16 (speed = 300 km/s) exists. ICME time and speed are different from Lindsay et al. 1999.

[e]CME onset time is incorrect in Lindsay et al. 1999. PVO position is not clear but East limb likely.

[f]ICME speed is different from Lindsay et al. 1999.

[g]CME time and date are different from Lindsay et al. 1999.

[h]ICME speed in km/s.

[i]He1 = Helios 1, PVO = Pioneer Venus Orbiter.

[j]CME speed in km/s.

[k]N - North, S - South, E - East, and W - West.

Table 2. List of CME - ICME events from SOHO and Wind apcecraft.

		ICME				CME					
No.	DOY	Date	UT	Vx[a]	Type[b]	Date	UT	Type[c]	Location[d]	speed[e]	T.T.
01	359	Dec. 24, 1996	0300	370	IMC	Dec. 19, 1996	1630	HCME	13°S,10°W	332	106.5
02	010	Jan. 10, 1997	0500	460	IMC	Jan. 06, 1997	1510	HCME	18°S,06°E	211	85.8
03	041	Feb. 10, 1997	0300	460	IMC	Feb. 07, 1997	0030	HCME	20°S,04°W	804	74.5
04	101	April 11, 1997	0600	470	Ej	April 07, 1997	1427	HCME	30°S,19°E	830	87.5
05	111	April 21, 1997	1500	400	IMC	April 16, 1997	0735	CME	22°S,04°E	247	127.4
06	135	May 15, 1997	1000	420	IMC	May 12, 1997	0630	HCME	21°N,08°W	306	75.5
07	159	June 08, 1997	2200	370	IMC	June 05, 1997	2255	CME	35°S,17°W	417	71.1
08	215	Aug. 03, 1997	1400	470	IMC	July 30, 1997	0445	CME	45°N,21°E	124	105.2
09	246	Sept. 03, 1997	1200	400	IMC?	Aug. 30, 1997	0130	HCME	30°N,17°E	427	106.5
10	265	Sept. 22, 1997	0300	470	IMC	Sept. 17, 1997	2028	HCME	30°N,10°W	487	102.5
11	274	Oct. 01, 1997	1800	475	EJ	Sept. 28, 1997	0108	HCME	22°N,05°E	355	88.9
12	283	Oct. 10, 1997	2300	430	IMC	Oct. 06, 1997	1528	CME	54°S,46°E	523	103.5
13	300	Oct. 27, 1997	1100	500	EJ?	Oct. 23, 1997	1126	HCME	22°N,01°E	493	95.6
14	311	Nov. 07, 1997	0530	450	IMC?	Nov. 04, 1997	0610	HCME	14°S,33°W	830	71.3
15	326	Nov. 22, 1997	2100	510	EJ	Nov. 19, 1997	1226	HCME	-	206	80.6
16	344	Dec. 10, 1997	1900	380	EJ	Dec. 06, 1997	1027	HCME	47°N,13°W	665	104.5
17	364	Dec. 30, 1997	1800	370	EJ	Dec. 26, 1997	0231	HCME	24°S,14°E	347	111.5
18	007	Jan. 07, 1998	0300	410	IMC?	Jan. 02, 1998	2328	HCME	47°N,03°W	446	99.5
19	049	Feb. 18, 1998	0800	400	EJ	Feb. 14, 1998	0700	HCME	22°S,20°E	275	97.0
20	063	March 04, 1998	1500	380	IMC	Feb. 28, 1998	1248	HCME	24°S,01°W	155	98.2
21	122	May 02, 1998	1300	600	IMC	April 29, 1998	1658	HCME	18°S,20°E	1016	68.0
22	124	May 04, 1998	1200	650	EJ	May 02, 1998	1406	HCME	15°S,15°W	1044	45.9
23	175	June 24, 1998	1530	520	IMC	June 21, 1998	0535	PH	15°N,30°W	307	81.9
24	292	Oct. 19, 1998	0430	420	IMC	Oct. 15, 1998	1004	HCME	22°N,01°W	239	90.4
25	311	Nov. 07, 1998	1100	530	EJ?	Nov. 04, 1998	0418	HCME	17°N,01°E	921	78.7
26	312	Nov. 08, 1998	0900	620	IMC	Nov. 05, 1998	2044	HCME	22°N,18°W	1123	60.2
27	069	March 10, 1999	1900	435	EJ?	March 07, 1999	0554	CME?	20°S,15°E	835	85.1
28	106	April 16, 1999	1930	460	IMC	April 13, 1999	0330	PH	16°N,00°E	282	88.0
29	111	April 21, 1999	0900	550	IMC?	April 17, 1999	0636	PH	25°S,05°W	362	98.4
30	126	May 06, 1999	0400	580	EJ?	May 03, 1999	0606	HCME	15°N,32°E	1147	69.9
31	188	July 07, 1999	0730	490	IMC?	July 03, 1999	1954	PH	18°N,55°W?	676	83.6
32	214	Aug. 02, 1999	1800	405	EJ?	July 31, 1999	1126	HCME	25°N,29°E	1079	54.6
33	233	Aug. 21, 1999	1600	500	IMC?	Aug. 17, 1999	1331	PH	21°N,28°E	953	98.5
34	294	Oct. 21, 1999	0930	410	EJ?	Oct. 18, 1999	0006	PH	30°S,15°E	222	81.4
35	042	Feb. 11, 2000	1000	480	IMC?	Feb. 08, 2000	0930	HCME	25°N,26°E	1080	72.5
36	043	Feb. 12, 2000	1500	540	IMC?	Feb. 10, 2000	0230	HCME	27°N,01°E	1009	60.5
37	052	Feb. 21, 2000	1800	400	EJ	Feb. 17, 2000	2130	HCME	29°S,07°E	550	92.5
38	090	March 30, 2000	0100	490	IMC?	March 25, 2000	2330	CME?	14°S,02°W	447	97.5
39	124	May 03, 2000	0600	560	EJ	April 29, 2000	0430	CME?	05°S,07°E	551	97.5
40	135	May 14, 2000	0300	490	IMC?	May 10, 2000	2006	PH	14°N,20°E	641	78.9
41	157	June 05, 2000	0030	470	EJ?	May 31, 2000	0806	HCME	28°N,04°E	396	112.4
42	160	June 08, 2000	1200	760	EJ	June 06, 2000	1554	HCME	21°N,15°E	1098	44.1
43	176	June 24, 2000	0800	580	EJ	June 20, 2000	0910	PH	23°N,23°W?	471	94.8
44	194	July 12, 2000	0000	540	IMC	July 07, 2000	1026	HCME	17°N,08°E	453	109.6
45	197	July 15, 2000	2200	1100	IMC	July 14, 2000	1054	HCME	22°N,07°W	1674	35.1
46	210	July 28, 2000	1500	460	EJ?	July 25, 2000	0330	HCME	06°N,08°W	532	83.5
47	213	July 31, 2000	2330	470	EJ?	July 28, 2000	1830	CME	25°N,72°E?	832	77.0

The abbreviations are DOY - day of the year; UT - universal time; T.T. - travel time in hours.
[a]X component of the speed (km/s) in GSE coordinates.
[b]IMC = Interplanetar Magnetic Cloud; EJ = Ejecta.
[c]HCME = Halo CME; PH = Partial Halo CME.
[d]? indicates most likely location.
[e]Plane of the sky projected CME speed (km/s).